Spectrochimica Acta Part A: Molecular and Biomolecular Spectroscopy 152 (2016) 637–644

Contents lists available at ScienceDirect

Spectrochimica Acta Part A: Molecular and Biomolecular Spectroscopy

journal homepage: www.elsevier.com/locate/saa

Controlling the exciton energy of zinc oxide (ZnO) quantum dots by changing the confinement conditions

Sergej Repp, Emre Erdem *

Albert-Ludwigs Universität Freiburg, Institut für Physikalische Chemie, Albertstrasse 21, 79104 Freiburg, Germany

HIGHLIGHTS

- Ability to control the particle size of ZnO with two different synthesis routes.
- Assignment of intrinsic defect centers in ZnO by EPR and PL spectroscopy.
- Exciton energy calculations by Brus theory.
- Observation of the quantum confinement effect during in situ precipitation reaction.

GRAPHICAL ABSTRACT

Monitoring quantum size effects by EPR spectra. With the aid of different chemical routes (SS, HydNa, HydLi) EPR spectra show drastic changes from bulk to nano-size samples.

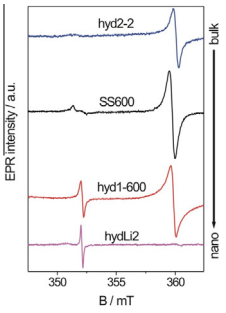

ARTICLE INFO

Article history:
Received 19 September 2014
Received in revised form 12 January 2015
Accepted 30 January 2015
Available online 11 February 2015

Keywords:
ZnO nanoparticles
Electron paramagnetic resonance (EPR) spectroscopy
Photoluminescence (PL) spectroscopy
Quantum dots

ABSTRACT

ZnO nanoparticles were synthesized by solid state and hydrolysis methods based on the conventional precipitation. In situ growth of ZnO nanoparticles were monitored by photoluminescence spectroscopy (PL). By the help of electron paramagnetic resonance (EPR) technique, detailed analysis of intrinsic defect structure of ZnO was given with respect to mean particle size. In nanoscale concentration of surface defects enormously increased and core defects reduced. In addition, blue-shift was observed in PL spectra at near-band-edge UV region due to e–h recombination. Calculation of band gap energies by the aid of Brus equation revealed consistent results with the experimental observations.

Introduction

Current research interest in nano-structured ZnO is motivated by novel applications as electrode material for dye-sensitized solar cells [1], light-emitting diodes [2], photoluminescence [3], thermoelectrics [4], printable electronics [5], varistors [6–8], sensors [8] or nano-generators [9]. All of these applications exploit the semiconducting properties of ZnO, which is a direct wide band-gap (3.37 eV) n-type semiconductor, and take advantage of the fact that desired material properties may be tailored by means of controlling not only the defect structure but also the band-gap energy by reducing the crystal/particle size or doping. Despite its advantages, the lack of fundamental knowledge about intrinsic defects and doping ions presents an obstacle to the development of practical devices which requires p-type conductivity for high performance. The difficulty to make reliable p-type ZnO is closely related to the intrinsic and extrinsic defects such as interstitials,

* Corresponding author.
E-mail address: emre.erdem@physchem.uni-freiburg.de (E. Erdem).

http://dx.doi.org/10.1016/j.saa.2015.01.110
1386-1425/

vacancies and doping ions, respectively. Although various ZnO compounds have been extensively investigated by many researchers over the last decades, there still exists controversy in various properties and some issues have even remained unclear. When the order of dimension is below 7 nm [10] in diameter the quantum size effects start to dominate the material system. Such nanoparticles have their size related, special characteristics and are sometimes called quantum dots (QD) [11,12]. The most striking feature of the nanoparticles is given by their chemical and physical properties which markedly differ from those of the bulk [13]. Several mechanisms exist which cooperate in achieving size effects. Thus, if the particle size falls short of the wavelength of photons, electrons and holes are spatially confined and energy levels become discrete. Furthermore, according to the quantization prescriptions applied to the *particle-in-box* idea of a solid, the electronic structure changes with particle size in an obvious way. As a consequence, light emission and absorption undergo pronounced frequency shifts with decreasing particle size. Promising characteristics of those materials is explainable by Bohr's atom model. The Bohr radius of an exciton (electron–hole pair) in a crystal can be treated in a similar vein. Excitons have their own material specific energy and radius and in case when the crystal volume decreases to nano-dimension then the exciton-radius becomes confined which is called quantum-size-effect. Due to this confinement the excitons gain energy thus readily makes a theoretical fundament to observe a blue-shifted irradiation from such nanomaterials. The effect of quantum confinement for different particle sizes was shown in Fig. 1. In particular, ZnO has a Bohr exciton radius of 2.34 nm [14,15] which shows quantum confinement effects.

Although metal ion doping and compound morphology play a decisive role to control materials properties, the synthesis method defines an additional, important role that markedly impacts nature and amount of intrinsic defects or impurities. In this work, we are aiming to provide a fundamental understanding of defects in undoped ZnO that could lead to reliable p-type ZnO. Recently, transition metal oxides with nanostructures have also attracted considerable interest in many areas of chemistry, physics and materials science. Compared to other metal oxide nanomaterials, ZnO displays novel nanostructures such as nano-wires [16], nano-rods [17], nano-tetrapods [18], nano-fibers [19], nano-walls [20], nano-tubes [21], nano-belts [22], nano-flowers [23] and nano-rings/nano-bows [24]. Consequently, ZnO-based nano-architectures have recently attracted significant attention since they open up ways for the development of new technological devices [25]. For such technological applications in semiconductor research, further improvement can be achieved by developing novel strategies to adjust the parameters of core–shell nano-materials and to control defect concentrations. Here, core–shell concept is applied in another manner than the two type material nano-architectures which have been described extensively by semiconductor society e.g., Klimov et al. for ZnSe/CdSe [26,27]. In the context of our research, core–shell model of ZnO can be explained as follows: the core contains negatively charged Zn vacancies and the shell is a surface medium containing high concentrations of defect complexes, in particular positively charged oxygen vacancies [28–30]. Electron paramagnetic resonance (EPR) and photoluminescence (PL) spectroscopy provide sensitive means to investigate corresponding features. In particular, EPR is well suited for understanding the role of defect centers since it provides a direct method to monitor different paramagnetic states of vacancies and paramagnetic metal ions and, thus, complements other experimental techniques such as PL. Furthermore, still controversially discussed phenomena, such as the role of intrinsic defects, the existence of room-temperature ferromagnetism [31,32], production of p-type ZnO semiconductors [33] and non-ohmic behavior of ZnO varistors [34] may be investigated.

The band structure of ZnO has been discussed over several decades, and there are still contradictions that prevent a unique band diagram. Contradictory defect assignments were given in different experimental and theoretical studies from the literature [35–37]. The contradicting assignments can be partly solved by analytical EPR in the framework of a core–shell model [29,30], which we have introduced in our previous works. Indeed, there are two main kinds of EPR signals in ZnO nano-materials. One originates from bulk defects and the other from surface defects. Due to their different environment each intrinsic defect center exhibits a specific g-factor in EPR spectra. In this model, the EPR signals at around $g \sim 1.96$ and around $g \sim 2.00$ are directly assigned to the core and the shell [38], respectively.

Bulk defects in ZnO can be identified according to a characteristic finger-print type EPR resonance at around $g \sim 1.96$. It is extremely difficult to resolve its g-anisotropy by standard cw-EPR at X- and Q-band microwave frequencies. The bulk defects are located at the hexagonal core of ZnO; thus they carry typical intrinsic properties of it. However, the real origin of the signal with a g-factor at around 1.96 is still unclear. This EPR signal is in general assigned to shallow donors [39,40] owing to a singly ionized oxygen vacancy defect (V_O^+) center [41–43]. However, it is sometimes also attributed to unpaired electrons trapped on oxygen vacancies [42], to shallow donor centers such as ionized impurity atoms in the crystal lattice of ZnO [44,45], or to free carriers in the conduction band [46]. In contrast to common conviction [47], there are reports supposing that the EPR signal at $g \sim 1.96$ may be due to one electron being weakly bound to ionized impurity atoms [48]. This implies that the electron from a shallow donor level is not completely delocalized into the conduction band but stays weakly bound to the original atoms, and behaves much like an electron in a hydrogen-like atom with a large Bohr exciton radius [48]. The irradiation with UV-light is expected to produce excitations and, once bound, the excitation would give rise to a paramagnetic signal at $g \sim 1.96$ suggesting that the signal is not related to oxygen vacancies [48].

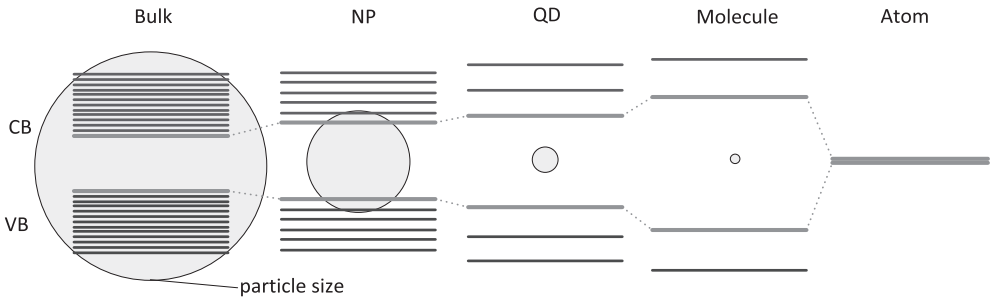

Fig. 1. Energy states of particles for different diameters (bulk, nanoparticles (NP), QD, molecule, atom) and the quantum confinement effects on their energy band gap. It is clearly distinguishable that QD have higher energy band gap energy and more discrete energy levels. VB: valance band, CB: conduction band.

The amount of surface-related defects enormously increases due to the increasing surface-to-volume ratio by size reduction to the nano-dimension. Since the surface of ZnO is an undefined structure, the defects in this region possess an electronic environment, which is difficult to describe and assign by EPR. In general, surface defects are detectable by EPR in a g range between 1.99 and 2.00. These defect centers indeed form defect complexes consisting of magnetically inequivalent anisotropic, axial or isotropic EPR signals. To resolve such overlapped or highly anisotropic signals is an extremely difficult issue. In the literature, various origins for the $g \sim 1.99$–2.00 signal have been pointed out. Zinc interstitials, negatively charged Zn vacancies, singly positively charged oxygen vacancies [49] or an unpaired electron trapped on an oxygen vacancy site [48] were reported. In some reports, the EPR spectrum of singly positively charged oxygen vacancies (sometimes called F^+-centers) is observed at a g-factor of ~1.99 only in irradiated ZnO samples under or after illumination and stable up to 400–450 °C annealing [58]. In very rare cases this signal has been assigned to Pb^{3+} deep donor impurities, with an Pb^{3+} isotropic EPR spectrum that has weak axial symmetry of the g-tensor around the c-axis with $g_z = 2.0133$ and $g_{x,y} = 2.0135$ [50]. Other contradictory assignments for the 1.99–2.00 signal, such as di- or tri-vacancy centers, shallow H donor, zinc vacancy related center, hole on an oxygen ion are summarized in an EPR-related review [51] and below in Table 1.

Optical properties of ZnO can be studied extensively by PL spectroscopy [37,61,62]. Numerous publications related to PL, both in the UV region and in the visible spectral range, can be found in the literature (refer Table 2). The origin and the mechanism underlying the luminescence centers is not really understood [37,62–65], and is frequently attributed to defect centers without compelling evidence (cf. Table 2). Thus, the nature of the blue (BL) [66], green (GL) [42,43,67], orange–red (ORL) [68], yellow (YL) [69] and red luminescence (RL) [70] bands remains controversial. In undoped ZnO, the GL band peak usually dominates the defect-related part of the PL spectrum [37,61], which was attributed to oxygen vacancies [71], zinc vacancies [72] and surface defects [29]. It is important to note here that the spectral position and the intensity of the defect-related emission band strongly depends on the synthesis of the material [73]. This is because the origin and also the concentration of intrinsic defects are in close relation with the synthesis procedure. Therefore, special emphasis should be given when comparing the PL of ZnO samples synthesized by different preparation methods.

In Table 2, possible origins for the visible band emission were summarized. Our previous PL results confirmed that the visible emission band is closely related to surface defects [28,29] and are also consistent with EPR results. However, in case of QD [96] and ZnO varistors [8], the UV and visible emission bands become more complicated and are still under discussion. In QD, due to the quantum-confinement effect, red or blue shifts might occur in PL emission lines [97]. Whereas in ZnO varistors, due to the effect of metal oxide additives, one may expect a obvious band gap increase or decrease, which might also affect the position of emission lines in PL [90].

Experimental

Synthesis of ZnO

Here, we specify two different preparation recipes called solid-state reaction and hydrolysis, which are based on the conventional precipitation. By introducing two different chemical routes we are aiming to investigate the effect of synthesis conditions on the defect structure of ZnO. The main advantages of these two methods are as follows: (i) reproducible way of preparation, (ii) cheap and eco-friendly and (iii) enables to adjust the mean particle size i.e., by annealing.

Solid state (SS) reaction

In this method following chemicals were used with the highest purity: zinc sulfate ($ZnSO_4$, Aldrich, purity 99%) and sodium hydroxide (NaOH (Roth, purity 99%)). NaOH and $ZnSO_4$ were grounded in a mortar with the molar ratio of 2:1 at room temperature (RT) for 30 min. After that, the solid mud was washed by millipore water. Afterwards the suspension was washed several times. The powder was dried 2 h at 80 °C in oven. Various sizes of ZnO nanoparticles were obtained by annealing the precursor at different temperatures (AT) ranging from 300 °C up to 600 °C. The annealing process was done as follows: RT (heating rate 8.3 °C/min) → AT (2 h) → free cooling to RT. Finally, the product was grounded.

The chemical equation in SS reaction is as follows:

$$ZnSO_4 + 2NaOH \rightarrow ZnO + Na_2SO_4 + H_2O \quad (1)$$

Hydrolysis (Hyd) reaction

Hydrolysis with NaOH (HydNa): Here, precursors were synthesized by using the following chemicals with the highest purity: zinc acetate ($Zn(OAc)_2$, Aldrich, purity 99.9%), sodium hydroxide (NaOH (Roth, purity 99%)) and ethanol (Analar Normapur, purity 99.99%). Two solutions with 0.1 M $Zn(OAc)_2$ and 0.55 M NaOH in ethanol were prepared separately. To increase the solubility of both chemicals in ethanol warm water bath at 60 °C were used. The precursors were left to cool down to RT and then the NaOH solution was dropwisely added into the stirred zinc solution. In this step the particle growth starts immediately and the particle size can be controlled by the reaction time. Due to the Ostwald ripening [98] it is a natural expectation that the longer the time is the larger the particle size reaches. Moreover, one may enhance the reaction rate by increasing the reaction temperature. To extract the ZnO yield from the solution we centrifuged it at 2500*g*. After ZnO yield were obtained it was subsequently washed four times with ethanol and dried under vacuum. The product was annealed as follows: RT (heating rate 8.3 °C/min) → 600 °C (2 h) → free cooling to RT. Finally, product was grounded by mortar. The chemical equation in HydNa reaction is as follows:

$$Zn(OAc)_2 + 2NaOH \rightarrow ZnO + 2NaOAc + H_2O \quad (2)$$

Hydrolysis with LiOH (HydLi): The synthesis is exactly the same as HydNa route however in this method instead of NaOH highly pure

Table 1
Various defect assignments of two distinct EPR signals at $g \sim 1.96$ and $g \sim 2.0$ for different ZnO systems.

g-Factor	System	Paramagnetic center
$g \sim 1.96$	Powder [43,49,52], single crystal [41,46,53–55], bulk crystal [56]	Shallow donor states [49,52,53], singly ionized V_O [43,48,52,57], V_{Zn} [41], distortion of the crystal lattice [46], impurities [48], delocalized donors [54], H-related shallow donor [55,56]
$g \sim 2$	Single crystal [58], powder [45,48,59], microcrystal [60]	V_{Zn} [45,58], O_2^- formation on the surface [52,60], V_O [48,59,60]

Table 2
ZnO luminescence data from literature. Recently reported lines emitted from ZnO and the proposed defect(s) causing the emission and their energies.

emission	energy (eV)	origin or transition mechanism
UV	3.34 [74], 3.27 [75], 3.34 [76], 3.36 [77, 78], 3.26 [79], 3.31 [80], 3.28 [81]	V_{Zn} [74], donor-bound excitonic (DBE) emission (D^0X) [76, 78], electron-hole recombination [77], free exciton recombination [79] [3, 82], free-to-bound transition [80], surface-bound ionized acceptor-exciton complexes [83], donor-acceptor pair transition [81], exciton-exciton collision process [82]
Violet 385-430 nm	2.98 [84]	Zn_i [85], H-related defect complexes [86], electron transition from a shallow donor level of Zn_i to the top level of valence band [84], lattice defects [82]
Blue 430-495 nm	2.8 [79], 3.06 [3], 2.9 [3], 2.82 [87], 2.77 [84]	V_O [79, 82, 88], V_{Zn} [3, 79], Zn_i [3, 82, 88], blue shift of green emission from surface V_O due to quantum confinement [89], O_i [89], surface defects [84, 88]
Green 495-570 nm	2.36 [43], 2.34 [90], 2.48 [75], 2.28 [77], 2.38 [67], 2.5 [79], 2.43 [78], 2.5 [91]	singly ionized V_O [43, 75, 78, 88, 91], Zn_i [3, 76, 88, 90], V_O [92] [61, 75] [67, 79], V_{Zn} [61, 92-94], donor acceptor pairs [61], surface localized states [77], antisite defects (O_{Zn}) [67, 94], transition between singly ionized V_O and a photoexcited hole [3]
Yellow 570-590 nm	2.17 [90], 2.21 [93], 2.2 [91], 2.13 [3], 2.14 [87], 2.19 [94]	O_i or other defect complexes [3, 90], V_O [3, 93], doubly ionized V_O [91], transition from shallow donor to a deep acceptor-V_{Zn} [94]
Orange 590-620 nm	2.07 [93], 1.97 [81]	O_i [85, 93, 94], excess local oxygen [81]
Red 620-750 nm	1.95 [78], 1.99 [71]	radiative transition between singly and doubly ionized V_{Zn} [78], Zn_i [85], O_i [71]
Visible broad emission	Between: 1.95-2.98	deep level defects [85] or vacancies [76, 93], point defects [95], surface bonded hydroxides [95], donor-acceptor complexes [95], electron-hole recombination of V_O [83]
IR	1.64 [92], 1.68 [81]	Radiative recombination of shallowly traped electrons with deeply trapped holes at O_i [92],

lithium hydroxide monohydrate ($LiOH{\cdot}H_2O$ (Aldrich, purity 99.99%)) was used. The chemical equation in HydLi reaction is as follows:

$$Zn(OAc)_2 + 2LiOH \cdot H_2O \rightarrow ZnO + 2LiOAc + 3H_2O \quad (3)$$

From the above mentioned synthesis routes following samples were obtained and assigned which are listed in Table 3.

Characterization methods

To check crystallinity, stoichiometry and the purity of the nanoparticles, X-ray diffraction (XRD) was applied with a STOE IPDS2 powder diffractometer equipped with a Cu Kα radiation source at a wavelength of $\lambda = 0.154$ nm. Samples were measured by Debye–Scherrer geometry. The morphology and further structural characterization ZnO particles were carried out using transmission electron microscopy (TEM) by using Carl Zeiss LEO 912 Omega instrument at acceleration voltage of 120 kV. TEM samples were prepared by evaporating a dilute suspension of ZnO particles on a carbon-coated copper grid. Photoluminescence (PL) spectra were recorded with a PerkinElmer LS 55 fluorescence spectrometer with 325 nm excitation and 5 nm excitation and emission slit width. A pulsed Xe lamp was used as excitation source. To remove spurious emission, a UG 5 filter was used. X-band (9.86 GHz) EPR measurements were performed with Bruker EMX spectrometer using a rectangular TE102 (X-band) resonator. The magnetic field was read using an NMR gaussmeter (ER 035M, Bruker); as a standard magnetic-field marker, polycrystalline DPPH with $g = 2.0036$ was used for the accurate determination of the resonance magnetic-field values.

Table 3
Assignments of the obtained ZnO particles by various methods and their expected particle dimension.

Sample assignment	Synthesis method	Particle dimension
SS600 and SS300	SS	Bulk and nano
Hyd1–600	HydNa	Bulk
Hyd2–2	HydNa	Nano or QD
HydLi2	HydLi	Nano or QD

Results and discussion

For the characterization of ZnO particles mainly XRD and TEM methods were used to determine the crystal structure and the

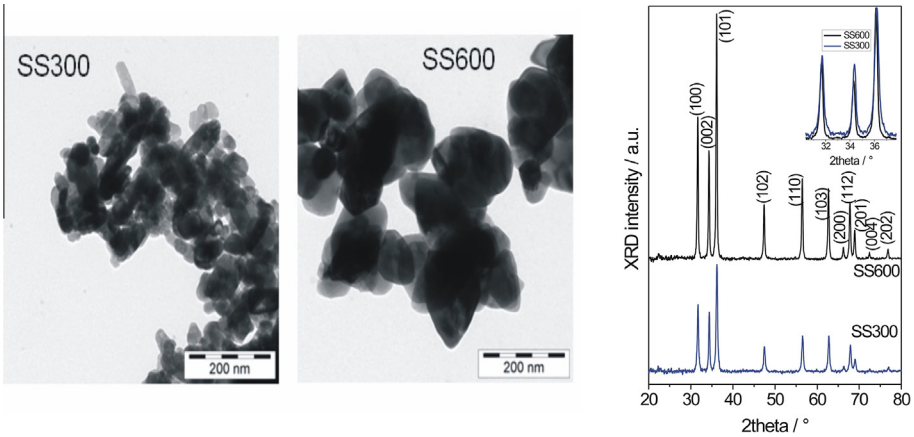

Fig. 2. TEM and XRD measurements of SS300 and SS600 samples synthesized by SS reaction and annealed at 300 and 600 °C, respectively. XRD diffraction pattern indicates formation of pure ZnO nanoparticles. Inset shows line broadening after normalization in XRD pattern in SS300 sample which indicates smaller particle size.

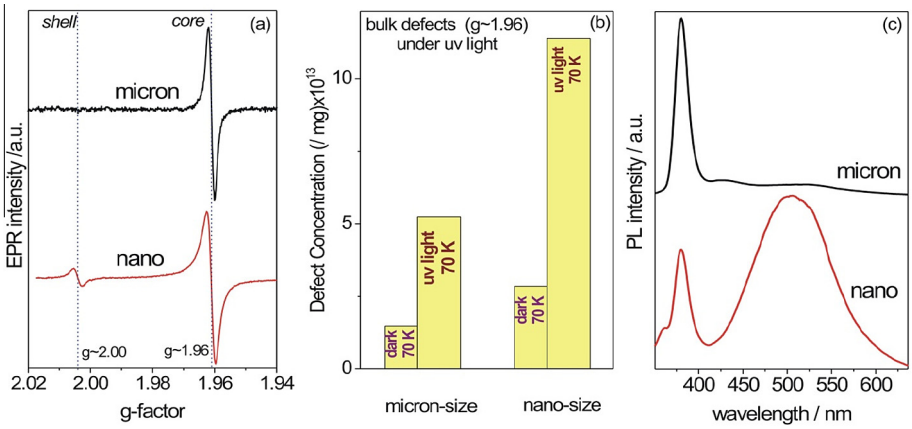

Fig. 3. (a) X-band EPR spectra for the micron- (bulk) and nano-size undoped ZnO at RT [38]. (b) Defect concentrations obtained from X-band EPR at 70 K for micron- and nano-sized ZnO, respectively both for the dark state and under UV light illumination [5]. The concentrations were determined from the bulk defects signal at $g \sim 1.96$ (cf. the EPR spectra inset) [5]. (c) PL spectra of micron- (bulk) and nano-size undoped ZnO [28].

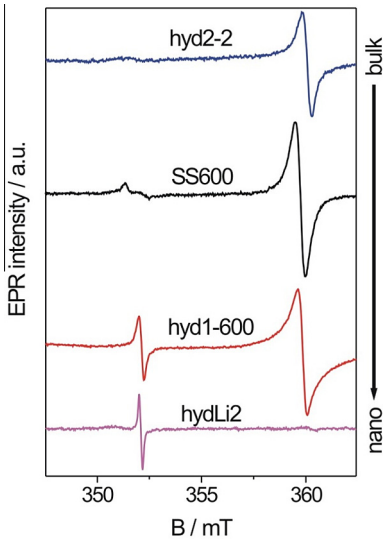

Fig. 4. Monitoring quantum size effects by EPR spectra. With the aid of different chemical routes (SS, HydNa, HydLi) EPR spectra show drastic changes from bulk to nano-size samples. The additional EPR peak at $g \sim 2$ (refer Fig. 3a) indicates nanosize crystal formation [38].

particle size. In Fig. 2 XRD and TEM results for SS synthesized ZnO samples were given and TEM results indicates 25–30 nm mean particle size for annealing temperature of 300 °C and 100–150 nm for 600 °C. XRD results also revealed pure diffraction pattern of ZnO and the expected broadening for nanosized samples.

In our previous EPR and PL works on ZnO material it has been introduced the core–shell model [29,30] and partly solved the defect assignment issue by designating the EPR signal at $g \sim 1.96$ to the defects on the core whereas signal at $g \sim 2.0$ to the defects on the surface. Correspondingly, UV-recombination emission peak around 380 nm and in PL visible band emission peak around 500–600 nm region in PL were correlated to the core and surface defects, respectively. Fig 3a and c shows the size effects in EPR and PL spectra due to core–shell model. On the other hand, the photosensitive features of core defect signal (EPR: $g \sim 1.96$, PL:

Table 4
Spin concentration in various ZnO samples obtained via spin counting procedure. The defect concentration on the core decreases by reducing the size whereas it increases on surface. Unit is spins/mg.

	Core	Shell
Hyd2–2	9.74×10^{14}	–
SS600	4.36×10^{14}	6.88×10^{13}
Hyd1–600	1.66×10^{14}	8.59×10^{13}
HydLi2	–	1.52×10^{14}

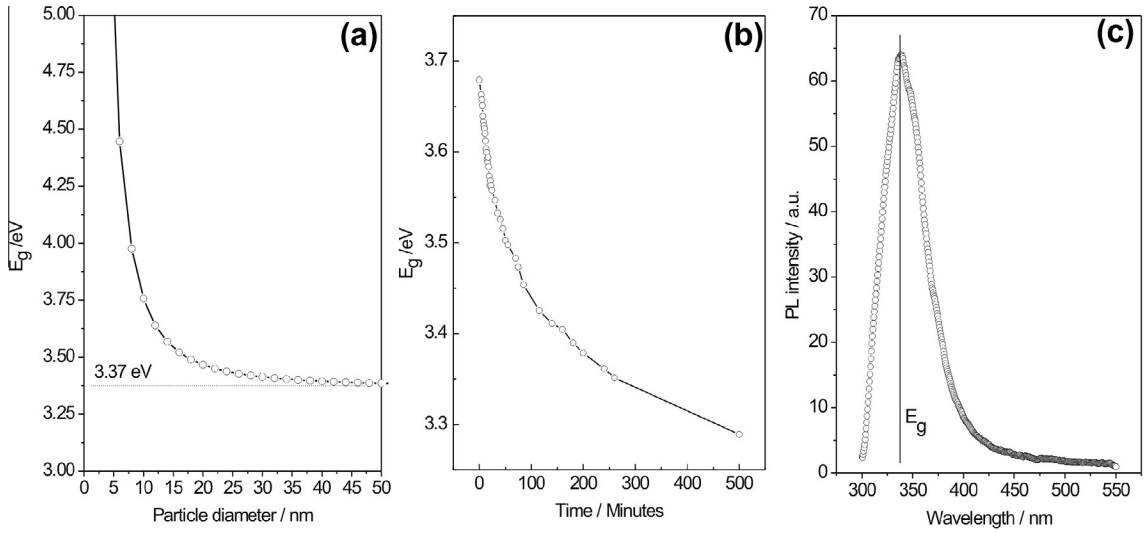

Fig. 5. (a) Band-gap energy calculation by the aid of Brus equation (Eq. (4)). (b) In-situ particle growth and band-gap measurement by in-situ PL measurement. (c) PL spectrum of ZnO QD synthesized by HydNa at 0 min.

Table 5
Summary of in-situ growth values of ZnO QDs.

Reaction time (min)	Emission wavelength (nm)	Band-gap energy (eV)	Calculated particle size (nm)
0	337	3.68	5.6
500	377	3.29	10.4

emission ~380 nm), e.g., enhancement after UV-light [99] (see also Fig. 3b), support that this signal can also safely be attributed to the electrons in conduction-band states, since UV-light can promote electrons into these states [36]. Fig. 3b shows the defect concentration in ZnO both for micron- and nano-sized samples after applying well known spin counting procedure [30,100]. It is clearly seen that nano-size samples have more defect centers than the micron-size. The defect concentrations were almost doubled under illumination with UV light. Independent from the origin of the defect center this result shows that by light excitation one can induce more intrinsic defects. The reason for that is the defects are stacking faults in the crystal lattice, e.g., vacancies, which represent additional electronic meta stable states. So by excitation those defect states would be populated and become EPR active.

In Fig. 4, strong size effects can be observed by EPR spectroscopy. By reducing the particle size the core signal (~360 mT) of bulk defects reduces and finally disappears, whereas the surface defect's signal becomes dominant. The quantitative values of the spin concentration have been summarized in Table 4 which are calculated by spin counting process [101]. In HydLi2 sample only the $g \sim 2.0$ defect signal left and this could be not only the paramagnetic surface defects but also it could be Li related defect centers [102,103]. To establish a relation between the EPR and PL results, the core–shell model for nanocrystalline ZnO is introduced previously [28–30]. By decreasing the particle size, the interior core becomes negatively charged due to an increase of V_{Zn}^{-} defects. V_{Zn}^{-} at Zn sites has spin quantum number $S = 1/2$ and therefore it reveals a typical single EPR line at $g \sim 1.96$. However, one could also attribute the same signal of bulk ZnO to the oxygen vacancies which are positively charged. According to our EPR and PL results, the core–shell model supports the negative charging of core and positive charging of the shell. This is mainly due to the decrease of the EPR signal at $g \sim 1.96$ and increase of defect related PL signal upon decreasing the crystal (core) size. Clearly, more oxygen vacancies are formed on the surface than in the core. The oxygen vacancies formed on the surface can trap either one (V_O^+) or two electrons (V_O) upon irradiation or excitation of the crystal with high-energy electrons or neutrons.

One of the alternative ways of controlling the particle size is doing in-situ PL measurements and monitoring the band-gap change simultaneously during the measurement by time. This enables us to relate the band gap variations to the particle size variation by well-known Brus equation which involves the particle size dependent photon excitation energy to determine the particle size:

$$E_g(R) = E_g(R \to \infty) + \frac{\hbar^2 \pi^2}{2R^2}\left(\frac{1}{m_e^*} + \frac{1}{m_h^*}\right) - \frac{1.786e^2}{4\pi\varepsilon_0\varepsilon_r R} \quad (4)$$

where m_e^* is the effective mass of the electron ($0.19m_e$), m_h^* is the effective mass of the hole ($0.8m_h$), R is the radius of the particle, ε_r is the dielectric constant of ZnO, and ε_0 is the permittivity of free space. The in-situ precipitation (HydNa) reaction was carried out in a cooled (0 °C) quartz cuvette in PL instrument with the excitation wavelength of 270 nm. In Fig. 5a Eq. (4) is plotted with respect to particle diameter versus band-gap energy which is schematically presented in Fig. 1. The electron–hole recombination energy, given in Fig 5b is decreasing with the growth time which supports the theoretical model of Brus, where the band-gap strongly increases with smaller particles. For a better understanding the PL spectrum of HydNa sample at 0 min were given in Fig. 5c and the growth values for 0 and 500 min were summarized in Table 5.

Conclusions

In this work, different synthesis methods namely, solid state and hydrolysis, were introduced for the production of ZnO and various particle sizes were obtained. Numerous ways of controlling particle sizes were given and by the aid of Brus equation one can estimate particle size from the energy-band gap energy calculation. Accordingly, by the help of in-situ PL measurements it is possible to observe the changes in the band-gap energy experimentally which gives correlation between EPR transitions and optical excitations. The estimation of particle size from Brus equation (Eq. (4)) can be enhanced by theoretical optimizations which needs advanced quantum mechanical approximation [104]. Samples synthesized by HydLi route showed characteristic

features to the direction of QD research and it will be discussed in future works. Overall, these results strongly suggest the interconnection between defects, synthesis route and particle size and experimental verification of quantum confinement. We believe that such an investigation will provide deep insight into the production of p-type conductivity, which is for a long time a dream achievement for undoped ZnO material.

Acknowledgments

This study was financially supported by the *Deutsche Forschunsgemeinschaft* (Grant: Er 662/1-2). We thank to Dr. M. Ade for XRD measurements and Dr. R. Thomann for TEM measurements. We gratefully acknowledge the support of Prof. S. Weber.

References

[1] K. Keis, E. Magnusson, H. Lindstrom, S.E. Lindquist, A. Hagfeldt, Solar Energy Mater, Solar Cells 73 (2002) 51–58.
[2] J. Bao, M.A. Zimmler, F. Capasso, X. Wang, Z.F. Ren, Nano Lett. 6 (2006) 1719–1722.
[3] A.B. Djurisic, W.C.H. Choy, V.A.L. Roy, Y.H. Leung, C.Y. Kwong, K.W. Cheah, T.K.G. Rao, W.K. Chan, H.T. Lui, C. Surya, Adv. Funct. Mater. 14 (2004) 856–864.
[4] Y. Kinemuchi, M. Mikami, K. Kobayashi, K. Watari, Y. Hotta, J. Electron. Mater. 39 (2009) 2059–2063.
[5] J.J. Schneider, R.C. Hoffmann, J. Engstler, S. Dilfer, A. Klyszcz, E. Erdem, P. Jakes, R.A. Eichel, J. Mater. Chem. 19 (2009) 1449–1457.
[6] T.K. Gupta, J. Am. Ceram. Soc. 73 (1990) 1817–1840.
[7] S.C. Pillai, J.M. Kelly, R. Ramesh, D.E. McCormack, J. Mater. Chem. C 1 (2013) 3268–3281.
[8] R. Baraki, P. Zierep, E. Erdem, S. Weber, T. Granzow, J. Phys. Condens. Matter 26 (2014) 115801.
[9] Z.L. Wang, J.H. Song, Science 312 (2006) 242–246.
[10] R. Viswanatha, S. Sapra, B. Satpati, P.V. Satyam, B.N. Dev, D.D. Sarma, J. Mater. Chem. 14 (2014) 661.
[11] A.P. Alivisatos, Science 271 (1996) 933–937.
[12] L.E. Brus, M. Bawendi, W.L. Wilson, L. Rothberg, P.J. Carroll, T.M. Jedju, M.L. Steigerwald, Am. Chem. Soc. 201 (1991) 409.
[13] R.P. Fynmann, Eng. Sci. 23 (1960) 22.
[14] P. Felbier, J. Yang, J. Theis, R.W. Liptak, A. Wagner, A. Lorke, G. Bacher, U. Kortshagen, Adv. Funct. Mater. 24 (2014) 1988.
[15] R.T. Senger, K.K. Bajaj, Phys. Rev. B 68 (2003) 045313.
[16] J.S. Reparaz, F. Guell, M.R. Wagner, A. Hoffmann, A. Cornet, J.R. Morante, Appl. Phys. Lett. 96 (2010) 053105.
[17] A.K. Srivastava, M. Deepa, K.N. Sood, E. Erdem, R.-A. Eichel, Adv. Mater. Lett. 2 (2011) (2011) 142–147.
[18] C. Zollfrank, C.R. Rambo, M. Batentschuk, P. Greil, J. Mater. Sci. 42 (2007) 6325–6330.
[19] D.Y. Lee, J.E. Cho, N.H. Cho, M.H. Lee, S.J. Lee, B.Y. Kim, Thin Sol. Films 517 (2008) 1262–1267.
[20] M. Mader, J.W. Gerlach, T. Hoche, C. Czekalla, M. Lorenz, M. Grundmann, B. Rauschenbach, Phys. Stat. Sol. RRL 2 (2008) 200–202.
[21] S.A. Morin, M.J. Bierman, J. Tong, S. Jin, Science 328 (2010) 476–480.
[22] Z.W. Pan, Z.R. Dai, Z.L. Wang, Science 291 (2001) 1947–1949.
[23] Y.J. Kim, J. Yoo, B.H. Kwon, Y.J. Hong, C.H. Lee, G.C. Yi, Nanotechnology 19 (2008) 315202.
[24] W.L. Hughes, Z.L. Wang, Appl. Phys. Lett. 86 (2005) 043106.
[25] M. Willander, O. Nur, Q.X. Zhao, L.L. Yang, M. Lorenz, B.Q. Cao, J. Zuniga Perez, C. Czekalla, G. Zimmermann, M. Grundmann, A. Bakin, A. Behrends, M. Al-Suleiman, A. El-Shaer, A. Che Mofor, B. Postels, A. Waag, N. Boukos, A. Travlos, H.S. Kwack, J. Guinard, D. Le Si Dang, Nanotechnology 20 (2009) 332001.
[26] L.P. Balet, S.A. Ivanov, A. Piryatinski, M. Achermann, V.I. Klimov, Nano Lett. 4 (2004) 1485.
[27] S.A. Ivanov, J. Nanda, A. Piryatinski, M. Achermann, L.P. Balet, I.V. Bezel, P.O. Anikeeva, S. Tretiak, V.I. Klimov, J. Phys. Chem. B 108 (2004) 10625.
[28] E. Erdem, J. Alloys Compd. 605 (2014) 34.
[29] H. Kaftelen, K. Ocakoglu, S. Tu, R. Thomann, S. Weber, E. Erdem, Phys. Rev. B 86 (2012) 014113.
[30] S.K.S. Parashar, B.S. Murty, S. Repp, S. Weber, E. Erdem, J. Appl. Phys. 111 (2012) 113712.
[31] J. Alaria, P. Turek, M. Bernard, M. Bouloudenine, A. Berbadj, N. Brihi, G. Schmerber, S. Colis, A. Dinia, Chem. Phys. Lett. 415 (2005) 337–341.
[32] I. Djerdj, G. Garnweitner, D. Arcon, M. Pregelj, Z. Jaglicic, M. Niederberger, J. Mater. Chem. 18 (2008) 5208–5217.
[33] S.B. Zhang, S.H. Wei, A. Zunger, Phys. Rev. B 63 (2001) 075205.
[34] A. Sedky, M. Abu-Abdeen, A.A. Almulhem, Physica B 388 (2007) 266–273.
[35] F. Boccuzzi, G. Ghiotti, A. Chiorino, J. Chem. Soc. 79 (1983) 1779–1789.
[36] A. Janotti, C.G.V. de Walle, Phys. Rev. B 76 (2007) 165202.
[37] U. Özgür, Y.I. Alivov, C. Liu, A. Teke, M.A. Reshchikov, S. Dogan, V. Avrutin, S.J. Cho, H. Morkoc, J. Appl. Phys. 98 (2005) 041301.
[38] P. Jakes, E. Erdem, Phys. Stat. Sol. RRL 5 (2011) 56–58.
[39] D.M. Hofmann, A. Hofstaetter, F. Leiter, H.J. Zhou, F. Henecker, B.K. Meyer, S.B. Orlinskii, J. Schmidt, P.G. Baranov, Phys. Rev. Lett. 88 (2002) 045504.
[40] S.B. Orlinskii, J. Schmidt, P.G. Baranov, C.D. Donega, A. Meijerink, Phys. Rev. B 79 (2009) 165316.
[41] S.M. Evans, N.C. Giles, L.E. Halliburton, L.A. Kappers, J. Appl. Phys. 103 (2008) 043710.
[42] N.Y. Garces, L. Wang, L. Bai, N.C. Giles, L.E. Halliburton, G. Cantwell, Appl. Phys. Lett. 81 (2002) 622–624.
[43] K. Vanheusden, W.L. Warren, C.H. Seager, D.R. Tallant, J.A. Voigt, B.E. Gnade, J. Appl. Phys. 79 (1996) 7983–7990.
[44] D.C. Look, R.L. Jones, J.R. Sizelove, N.Y. Garces, N.C. Giles, L.E. Halliburton, Phys. Stat. Sol. a 195 (2003) 171–177.
[45] S. Moribe, T. Ikoma, K. Akiyama, Q.W. Zhang, F. Saito, S. Tero-Kubota, Chem. Phys. Lett. 436 (2007) 373–377.
[46] V.A. Nikitenko, J. Appl. Spectrosc. 57 (1992) 367–385.
[47] C. Gonzalez, D. Block, R.T. Cox, A. Herve, J. Cryst. Growth 59 (1982) 357–362.
[48] V. Ischenko, S. Polarz, D. Grote, V. Stavarache, K. Fink, M. Driess, Adv. Funct. Mater. (2005) 1945–1954.
[49] M. Kakazey, M. Vlasova, M. Dominguez-Patino, G. Dominguez-Patino, T. Sreckovic, N. Nikolic, Sci. Sinter. 36 (2004) 65–72.
[50] L.S. Vlasenko, Physica B 404 (2009) 4774–4778.
[51] B.K. Meyer, H. Alves, D.M. Hofmann, W. Kriegseis, D. Forster, F. Bertram, J. Christen, A. Hoffmann, M. Strassburg, M. Dworzak, U. Haboeck, A.V. Rodina, Phys. Stat. Sol. B 241 (2004) 231–260.
[52] Y. Hu, H.J. Chen, J. Nanopart. Res. 10 (2008) 401–407.
[53] S.B. Orlinskii, J. Schmidt, P.G. Baranov, V. Lorrmann, I. Riedel, D. Rauh, V. Dyakonov, Phys. Rev. B 77 (2008) 115334.
[54] W.E. Carlos, E.R. Glaser, D.C. Look, Physica B 308 (2001) 976–979.
[55] M.A. Gluba, F. Friedrich, K. Lips, N.H. Nickel, Superlat. Microstruct. 43 (2008) 24–27.
[56] D.M. Hofmann, D. Pfisterer, J. Sann, B.K. Meyer, R. Tena-Zaera, V. Munoz-Sanjose, T. Frank, G. Pensl, Appl. Phys. A 88 (2007) 147–151.
[57] Y. Jeong, C. Bae, D. Kim, K. Song, K. Woo, H. Shin, G. Cao, J. Moon, ACS Appl. Mater. Interfaces 2 (2010) 611–615.
[58] D. Galland, A. Herve, Sol. Stat. Commun. 14 (1974) 953–956.
[59] A. Pöppl, G. Völkel, Phys. Stat. Sol. a 121 (1990) 195–204.
[60] B.L. Yu, C.S. Zhu, F.X. Gan, Y.B. Huang, Mater. Lett. 33 (1998) 247–250.
[61] Y. Gong, T. Andelman, G.F. Neumark, S. O'Brien, I.L. Kuskovsky, Nanoscale Res. Lett. 2 (2007) 297–302.
[62] A. Janotti, C.G. Van de Walle, Rep. Prog. Phys. 72 (2009) 126501.
[63] A.B. Djurisic, Y.H. Leung, Small 2 (2006) 944–961.
[64] A.B. Djurisic, Y.H. Leung, K.H. Tam, L. Ding, W.K. Ge, H.Y. Chen, S. Gwo, Appl. Phys. Lett. 88 (2006) 103107.
[65] A.B. Djurisic, Y.H. Leung, K.H. Tam, Y.F. Hsu, L. Ding, W.K. Ge, Y.C. Zhong, K.S. Wong, W.K. Chan, H.L. Tam, K.W. Cheah, W.M. Kwok, D.L. Phillips, Nanotechnology 18 (2007) 095702.
[66] H. Zeng, G. Duan, Y. Li, S. Yang, X. Xu, W. Cai, Adv. Funct. Mater. 20 (2010) 561–572.
[67] Z.G. Wang, X.T. Zu, S. Zhu, L.M. Wang, Physica E 35 (2006) 199–202.
[68] G.H. Du, Y.Q. Yang, T.B. Li, B.S. Xu, J. Mater. Sci. 45 (2010) 1464–1468.
[69] M.A. Reshchikov, J.Q. Xie, B. Hertog, A. Osinsky, J. Appl. Phys. 103 (2008) 103514.
[70] J.H. Cai, G. Ni, G. He, Z.Y. Wu, Phys. Lett. A 372 (2008) 4104–4108.
[71] N.H. Alvi, K. ul Hasan, O. Nur, M. Willander, Nanosci. Res. Lett. 6 (2011) 7.
[72] F. Tuomisto, K. Saarinen, D.C. Look, G.C. Farlow, Phys. Rev. B 72 (2005) 647413.
[73] D. Li, Y.H. Leung, A.B. Djurisic, Z.T. Liu, M.H. Xie, S.L. Shi, S.J. Xu, W.K. Chan, Appl. Phys. Lett. 85 (2004) 1601–1603.
[74] A. Zubiaga, J.A. Garcia, F. Plazaola, F. Tuomisto, K. Saarinen, J. Zuniga Perez, V. Munoz-Sanjose, J. Appl. Phys. 99 (2006) 053516.
[75] Y.J. Choi, H.H. Park, J. Mater. Chem. C 2 (2014) 98–108.
[76] J. Li, H. Fan, X. Chen, Z. Cao, Colloids Surf. A 349 (2009) 202–206.
[77] P.K. Sharma, A.C. Pandey, G. Zolnierkiewicz, N. Guskos, C. Rudowicz, J. Appl. Phys. 106 (2009) 094314.
[78] J.P. Biethan, V.P. Sirkeli, L. Considine, D.D. Nedeoglo, D. Pavlidis, H.L. Hartnagel, Mater. Sci. Eng. B 177 (2012) 594–599.
[79] G. Xiong, U. Pal, J.G. Serrano, K.B. Ucer, R.T. Williams, Phys. Stat. Sol. C 3 (2006) 3577–3581.
[80] M. Schirra, R. Schneider, A. Reiser, G.M. Prinz, M. Feneberg, J. Biskupek, U. Kaiser, C.E. Krill, K. Thonke, R. Sauer, Phys. Rev. B 77 (2008) 125215.
[81] A. Kumar, S. Jeedigunta, I. Tarasov, S. Ostapenko, AZo J. Mater. Onl. 6 (2010) 1.
[82] S.K. Panda, N. Singh, J. Hooda, C. Jacob, Cryst. Res. Technol. 43 (2008) 751–755.
[83] G. Kiliani, R. Schneider, D. Litvinov, D. Gerthsen, M. Fonin, U. Ruediger, A. Leitenstorfer, R. Bratschitsch, Opt. Express 19 (2011) 1641–1647.
[84] S.K. Mishra, R.K. Srivastava, S.G. Prakash, R.S. Yadav, A.C. Panday, Opt. Electron. Rev. 18 (2010) 467–473.
[85] M. Willander, O. Nur, J.R. Sadaf, M.I. Qadir, S. Zaman, A. Zainelabdin, N. Bano, I. Hussain, Materials 3 (2010) 2643–2667.
[86] C. Chen, Y. Lu, H. He, M. Xiao, Z. Wang, L. Chen, Z. Ye, ACS Appl. Mater. Interfaces 5 (2013) 10274–10279.
[87] M.L. Kahn, T. Cardinal, B. Bousquet, M. Monge, V. Jubera, B. Chaudret, Chem. Phys. Chem. 7 (2006) 2392–2397.
[88] A.J. Reddy, M.K. Kokila, H. Nagabhushana, J.L. Rao, C. Shivakumara, B.M. Nagabhushana, R.P.S. Chakradhar, Spectrochim. Acta A 81 (2011) 59–63.

[89] L.-L. Han, L. Cui, W.-H. Wang, J.-L. Wang, X.-W. Du, Semicond. Sci. Technol. 27 (2012) 065020.
[90] M.S. Ramanachalam, A. Rohatgi, W.B. Carter, J.P. Schaffer, T.K. Gupta, J. Electron. Mater. 24 (1995) 413–419.
[91] S.K. Chaudhuri, M. Ghosh, D. Das, A.K. Raychaudhuri, J. Appl. Phys. 108 (2010) 064319.
[92] M. Wang, Y. Zhou, Y. Zhang, E.J. Kim, S.H. Hahn, S.G. Seong, Appl. Phys. Lett. 100 (2012) 101906.
[93] V.P. Singh, D. Das, C. Rath, Mater. Res. Bull. 48 (2013) 682–686.
[94] X. Zhang, S. Hou, H. Mao, J. Wang, Z. Zhu, Appl. Surf. Sci. 256 (2010) 3862–3865.
[95] L.Y. Zhang, L.W. Yin, C.X. Wang, N. Lun, Y.X. Qi, D. Xiang, J. Phys. Chem. C 114 (2010) 9651–9658.
[96] G. Kiliani, R. Schneider, D. Litvinov, D. Gerthsen, M. Fonin, U. Rudiger, A. Leitenstorfer, R. Bratschitsch, Opt. Express 19 (2011) 1641–1647.
[97] K.F. Lin, H.M. Cheng, H.C. Hsu, L.J. Lin, W.F. Hsieh, Chem. Phys. Lett. 409 (2005) 208–211.
[98] P. Dagtepe, V. Chikan, J. Phys. Chem. C 114 (2010) 16263–16269.
[99] L. Schneider, S.V. Zaitsev, W. Jin, A. Kompch, M. Winterer, M. Acet, G. Bacher, Nanotechnology 20 (2009) 135604.
[100] C.V. Pham, M. Krueger, M. Eck, S. Weber, E. Erdem, Appl. Phys. Lett. 104 (2014) 132102.
[101] G.R. Eaton, S.S. Eaton, D.P. Barr, R.T. Weber, Quantitative EPR, Springer, Berlin, 2010.
[102] C. Rauch, W. Gehlhoff, M.R. Wagner, E. Malguth, G. Callsen, R. Kirste, B. Salameh, A. Hoffmann, S. Polarz, Y. Aksu, M. Driess, J. Appl. Phys. 107 (2010) 024311.
[103] O.F. Schirmer, J. Phys. Chem. Sol. 29 (1968) 1407.
[104] A.D. Yoffe, Adv. Phys. 51 (2002) 799–890.